Rovira Más, F.; Chatterjee, I.; Sáiz Rubio, V. (2015). The role of GNSS in the navigation strategies of cost-effective agricultural robots. Computers and Electronics in Agriculture. 112:172-183. doi:10.1016/j.compag.2014.12.017.

The role of GNSS in the navigation strategies of cost-effective agricultural robots

Francisco Rovira-Más[1,*], Ishani Chatterjee[2], Verónica Sáiz-Rubio[1]

[1] *Agricultural Robotics Laboratory, Universidad Politécnica de Valencia, Camino de Vera s/n, 46022 Valencia, Spain*

[2] *Department of Agricultural and Food Engineering, Indian Institute of Technology, Kharagpur, India*

[*] *Corresponding author*: Francisco Rovira-Más; Tel: +34 963877291; email: frovira@dmta.upv.es

Abstract

The current state of automation technology has led to a growing interest in the design and development of new use-case agricultural robots that can provide effective solutions to the challenges that agriculture is facing in industrialized countries, especially those derived from labor shortage and ever-increasing production costs. The advent of autonomous moderate-size machines in the field appears as a prospective way of promoting the sustainable production of food in Europe, Japan, and North America. However, there exist important obstacles to the broad expansion of autonomous robots in the field; reliability, safeguarding, system complexity, and cost-efficiency in particular rank high among the impediments to overcome before prototypes move into the production stage. Robot navigation is essential for the successful deployment of autonomous machines in conventional farms, as a minimum level of safety has to be granted at the same time that navigation engines cannot be too sophisticated for solutions to compete with current equipment. In such compromise, global navigation satellite systems play a key role due to its wide range of solutions, and an important number of limitations. In this research, a variety of experiments were conducted to determine the scope of GNSS solutions as a principal component of the navigation system of novel farm robots. Results showed that regardless of the quality of the receiver used, multipath and

other uncontrollable errors eventually occur in the field, and therefore signal consistency must be continuously checked by the robot's navigation engine. Different strategies based on the meticulous analysis of NMEA strings, the optimal combination of GGA and VTG messages, and the trajectory-based redundant estimation of robot planar states are proposed to enhance the integration of GNSS measurements in the navigation engine of agricultural robots.

Keywords

Agricultural robotics; farm robots; GNSS; navigation strategies; autonomous navigation

1. Introduction

The accessibility of GNSS (Global Navigation Satellite Systems) for civil applications has revolutionized the way we farm today. Precision farming packages are available from most of the major manufacturers of agricultural equipment, and site-specific management is gaining acceptance on a global scale. Global positioning systems are an essential technology for agriculture not only for research but also in practical use (Chosa et al., 2007). Therefore, disregarding global positioning systems when building the navigation strategies of field robots, especially those performing agricultural tasks, would probably lead to limited solutions and an inefficient use of available resources. As a matter of fact, nearly all robots designed for outdoor operations —except planetary rovers– incorporate some sort of global navigation, and the trend has been moving upward since the cancelation of selective availability in 2000. A study of patents on intelligent vehicles and automatic navigation for the period 1985-2008 (Rovira-Más, 2009) reveals that eighty percent of the patents related to GPS (Global Positioning System) were published after 2000. The growing interest in satellite navigation for agricultural applications has motivated the development of ASABE Standard X587 (ASABE, 2010), which focuses on performance of positioning devices subjected to ground-based

agricultural field operations.

The easy access to GNSS information, however, contrasts with the difficulty of assuring long-term robust and reliable measurements, especially for crucial dynamic states such as heading and speed. GPS dynamic accuracy depends on the travel direction due to satellite geometry in mid-latitude areas where satellite distribution is uneven because of the lack of satellites in the northern skies (Wu et al., 2006). Specifically, substantial differences have been found between north dilution of precision (NDOP) and east DOP (EDOP), being NDOP usually higher than EDOP. Likewise, the cross-track DOP (XDOP) perpendicular to the travel direction increases as the reference axis changes from 0º to 90º, which explains the direction dependency of cross-track errors. GPS-based velocity estimation, on the other hand, usually provides positive results as long as there are no satellite coverage discontinuities provoked by overhead structures, electromagnetic interferences onboard are kept low, and multipath signal reception is reduced as much as possible, especially reflections caused by water bodies (Cocco and Rapuano, 2007).

Given that GNSS provides useful navigation information when estimates are reliable, but reliability cannot be always granted in general terms, farm robots must be endowed with an advanced architecture in such a way that the navigation algorithms embedded in the robot always make an optimized use of available data in real time. The *Robotra* tillage robot developed in 1997 (Kondo et al., 2011), for example, features an architecture based on a main computer that receives GNSS navigation data through an RS-232C bus and a complementary vehicle controller that receives feedback information from the robot sensors and exerts navigational control commands to actuate the steering mechanism, the gear shift, the throttle, and the independent brakes. Safety was tackled with three fundamental actions occurring concurrently: a feeling bumper, a contactless obstacle detector, and a remote control stop switch. The navigation strategy for the

Robotra robot consists of a pre-planned path achieved by combining an RTK-GPS, and inertial measurement unit (IMU), and a geomagnetic direction sensor. The general architecture for agricultural vehicles proposed by Rovira-Más (2010) considers that the intelligent behaviors embedded in farm robots may follow a three-layer classification of tasks, where the task with the highest priority is safety, followed by the other two; namely, the information layer and the machine actuation layer. The information layer handles all the data coming from the sensors whereas the actuation layer executes orders and commands. In order to keep these three layers continuously iterating, a system architecture is necessary, and four structural sub-systems are proposed as its building blocks; local perception, global localization, actuation and control, and data processing and storage. Advanced navigation, therefore, requires the proper functioning of the four of them. The particular architecture developed for the *Robotra* tillage tractor easily fits the general architecture defined by Rovira-Más (2010). In a similar fashion, Emmi et al. (2014) propose an architectural design based on three main modules devoted to sensing, acting, and decision making, being GNSS included in the sensing module. This architecture has been successfully tested for weed control in corn fields, where an off-road vehicle was programmed to follow a pre-defined path indicated by GPS waypoints, although perception was necessary at row initiation due to the uncertainty in determining the starting point.

All the architectures described above integrate GNSS as one of their main components, and the majority of field applications reported by the agricultural sector use global-based data for vehicle navigation, typically combined with other sensors. Van Begeijk et al. (1998), for instance, estimated heading redundantly with a GPS receiver and an electronic flux-gate compass. The compass turned out to be the weakest point in the positioning system in terms of accuracy and mounting possibilities, and consequently,

trajectory-based GPS heading resulted more precise than compass heading for forward velocities greater than 1 m/s. Field work demonstrated the strong dependency of heading calculation on traveling speed, and showed that compasses are difficult to mount on off-road vehicles, as 1.5 m clearance from iron and steel parts is at least necessary to avoid magnetic disturbances. The actuation of an autonomous mechanical weeder (Nørremark et al., 2008) involved the global referencing of individual plants as well as that of the weeding robot, where the forward velocity was supplied by an onboard RTK-GPS receiver and the orientation of the route was directly estimated from a sequence of waypoints. The strong dependence of heading estimation on traveling speed noticed by Van Begeijk et al. (1998) led Anderson and Bevly (2010) to propose velocity-based course measurements from the combination of a GPS and a low-cost gyroscope through a Kalman-based estimator. The complexity of adding a gyroscope through a model-based estimator allowed the measurement of such vehicle states as sideslip and yaw rate, in addition to habitual heading and speed. Inertial sensors, however, have not been the only assistance to strengthen the navigation skills of autonomous vehicles, as perception sensors have resulted helpful to assure positioning data when GPS signals are attenuated or blocked, as the laser-based range-domain integration of Joerger and Pervan (2006), or the automatic weed detector developed by Emmi et al. (2014), which detected the center of crop rows at the headland with machine vision but continued the pre-established path defined by GPS waypoints.

The use of GNSS permeates through most of the solutions devised in the last two decades for robot navigation outdoors, although a large number of them are either too unreliable or too expensive for their practical integration in farm robots. Although RTK-GPS provides the highly accurate positioning needed to control field machinery and farm work precisely, it is too expensive to be widely used in farm machinery. A positioning

system is therefore required that is less expensive and equipped to handle centimeter accuracy; however, the accuracy of a system in practical use is unclear (Chosa et al., 2007). Given that obtaining accurate velocity information has traditionally involved expensive solutions such as optical sensors and RTK-GPS, Serrano et al. (2004) have proposed estimating velocity from the time-differential method using a stand-alone single-frequency receiver without resolving carrier phase ambiguities. This solution, however, requires the application of post-processing software and the availability of carrier and Doppler measurements, which limit the needs for real-time navigation data of farm robots and complicate the practical integration of GNSS receivers in the field as wave functions must be acquired and processed rather than standard GNSS messages such as those shown in Fig. 1. The problems found with Serrano's approach caused by the need of knowing carrier phase measurements and the receiver positions before and after each epoch, which make the method unsuitable for real-time applications, were circumvented by an algorithm that uses receiver position at epoch t and satellite positions at epoch $t + \Delta t$ (Ding and Wang, 2011). However, this method also uses carrier phase and wavelength in its formulation as well as time ambiguity and clock biases, all of them parameters of difficult access for commercial users. In addition, given that Ding and Wang based their approach on single point positioning (SPP), ionosphere and troposphere models had to be used to compensate raw measurements, which can be efficiently avoided by using a differential receiver (DGPS), perfectly compatible with the assumption of cost-efficiency held in this research. Chosa et al. (2007) proved that, after error compensation, accurate positioning is possible with a stand-alone single-frequency GNSS receiver, where velocity can be derived by measuring the Doppler shift of carrier waves.

The main objective pursued with this research is to determine the role of GNSS information in the navigation strategies of agricultural robots according to the equilibrium

between reliability and cost-efficiency, using standard GNSS messages as positioning sensor inputs for the system integration. As a result, measurements and analyses of the raw carrier waves emitted by satellites will not be considered in the algorithms and solutions developed hereafter.

2. Methodology

When navigation strategies are to be defined, especially if local and global data are going to be fused, the selection of an advantageous coordinate system is of primary importance. The local tangent plane, commonly known as easting-northing, provides an ideal setting for fusing vehicle states measured with sensors of diverse nature (Rovira-Más et al., 2010). Table 1 correlates the most common navigation parameters used by field robots with conventional sensors of widespread use in off-road vehicles. Notice the degree of redundancy inherent in the table in general, as well as the particular case of GNSS where some parameters can also be redundantly estimated only with GNSS messages. In light of this concurrence of —a priori– equivalent measurements, some sort of hierarchy needs being established before data are processed by the navigation engine of the robot. The point of this paper is ranking GNSS information through Table 1 in such a way that only the most reliable estimates get to the navigation algorithms. This prioritization will necessarily change with the surrounding conditions, and assessments must be performed iteratively in real time.

Table 1. Navigation data sources for agricultural robots.

	Position	**Time**	**Velocity**	**Heading (yaw)**	**Attitude (pitch/roll)**
GNSS	Direct GGA string	Direct GGA string	Direct VTG st. Derived seq.	Direct VTG st. Derived seq. Two receivers	Two receivers
Gyroscope/IMU	Dead reck.	--	Angular (yaw rate)	Through 1 integration	--
Doppler-Radar	Dead reck.	--	Direct	--	--

Compass	--	--	--	Direct	--
Machine Vision	Local, derived from features	--	Derived Video flow	Local, derived from features	--

Abbreviations: st→string; seq→sequence; reck→reckoning; IMU→Inertial Measurement Unit

Table 1 shows that Doppler-based radar is basically used to provide an independent estimate of ground speed, gyroscopes and compasses are appropriate to know the heading, and machine vision is practically limited to local perception, given that dead reckoning is inappropriate for off-road vehicles and environments where wheel slippage is usual. The capacity of GNSS, however, is much broader, and practically all the parameters listed in Table 1 can be estimated —with more or less precision– from this unique source. The objective is determining when each source should be given more or less weight based on its real-time reliability. The use of two separate receivers in one vehicle to determine yaw, pitch, and roll requires purchasing two receivers of high performance such that slight changes in attitude are precisely measured. This option, however, is against the cost-efficiency premise stated in this study and therefore will not be taken into account at this stage. Further studies may include the estimation of pitch and roll.

According to Table 1, position and time is directly transmitted by GGA NMEA (National Marine Electronic Association Standard 0183) strings, whereas velocity and heading are directly conveyed by VTG strings. GNSS receivers, therefore, broadcast these four basic parameters in two different strings that may be recorded simultaneously. Figure 1 specifies the morphology of NMEA strings for GNSS messages.

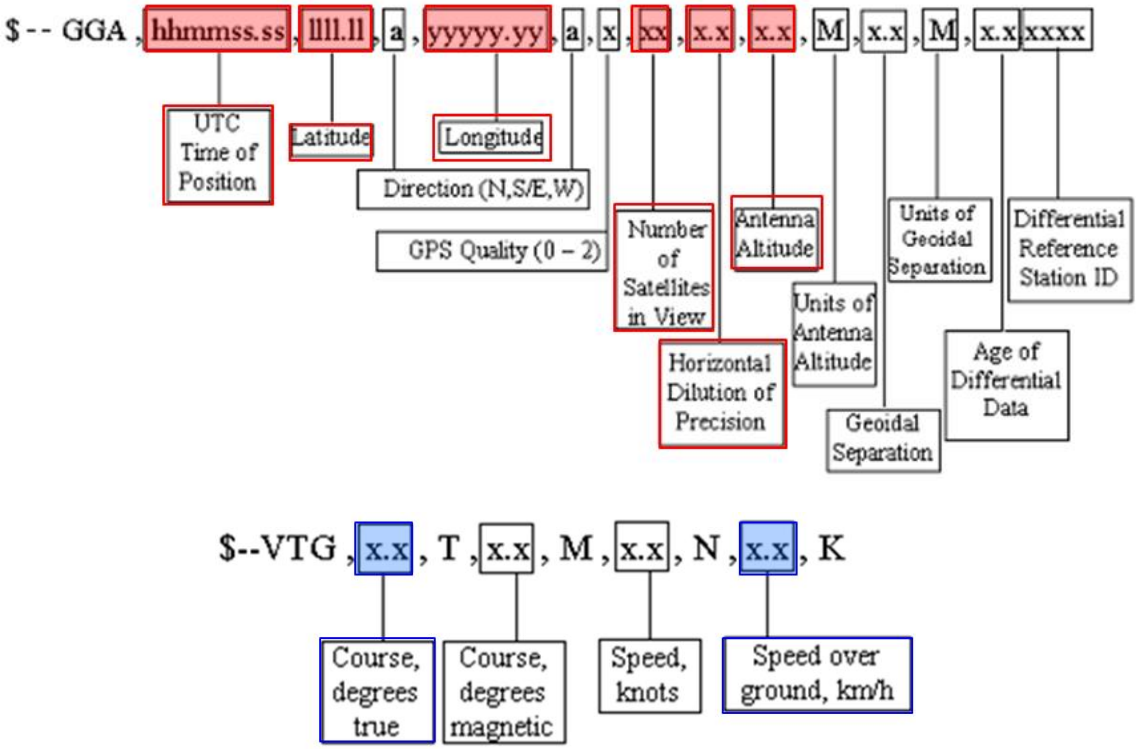

193

194

195 Figure 1. Morphology of NMEA strings: GGA (a) and VTG (b).

196 Due to the fact that GGA strings (Fig. 1a) provide position and time
197 simultaneously, instant velocity may be derived from a sequence of consecutive points.
198 However, it is important to keep in mind that this way of calculating speed differs from
199 the way speed is calculated in VTG strings (Fig 1b), as direct calculations of speed are
200 based on Doppler measurements, and are normally superior to position-based
201 calculations. The procedure to derive heading and speed (in a plane) from a sequence of
202 consecutive points defined by GGA strings (Fig. 1a), previously transformed to the local
203 tangent plane, can be summarized as follows. All the points recorded in the field by the
204 GNSS receiver constitute a set $\boldsymbol{T}$ of mathematical objects defining the trajectory of a robot
205 in time and 2D (planar) space. The specific points of the trajectory used at a given moment
206 to calculate heading and speed form a subset $\boldsymbol{S}$ of $\boldsymbol{T}$. In a formal definition, let $\boldsymbol{T} = \{1, 2,$
207 $\ldots, m\}$ be the set of the indices of points defining the trajectory of a robot in the field, and
208 Let $\boldsymbol{S} = \{1, 2, \ldots, h+1\} \subset \boldsymbol{T}$ be the subset of the indices of points used in the calculation
209 of heading or speed and forming the calculation matrix M_s. The calculation matrix M_s

composed from the elements of ***S*** will be dynamic —i. e. changing with time– and its dimension will be *h*+1 x 3. A general formulation of the calculating matrix for any given point *k* is shown in Eq. 1, where *k* is the point in the sequence ***T*** being calculated, E is the east coordinate (m), N is the north coordinate (m), and *t* is the receiver time (s). The size (*m*) of set ***T*** depends on the traveling speed and the length of the trajectory traced by the robot in the field, both imposed by each particular task. Therefore, the size of ***T*** is generally determined by external factors. However, the size of subset ***S*** is an important parameter setup beforehand, which in practice influences the estimation of heading and velocity from GNSS positions.

$$M_s(k) = \begin{bmatrix} E_k & N_k & t_k \\ E_{k-1} & N_{k-1} & t_{k-1} \\ E_{k-2} & N_{k-2} & t_{k-2} \\ \bullet & \bullet & \bullet \\ \bullet & \bullet & \bullet \\ \bullet & \bullet & \bullet \\ E_{k-h} & N_{k-h} & t_{k-h} \end{bmatrix}_{h+1\,x\,3} \quad ;k > h; \quad t_k > t_{k-1} > ... > t_{k-h} \qquad (1)$$

The analysis of a point sequence ***T*** belongs to discrete mathematics, which focus on mathematical structures that are discrete in nature and whose components can be enumerated by integers, constituting a countable set that can be finite or infinite. The set ***T*** that defines the robot's trajectory can be saved by the onboard computer and therefore is finite and bounded by *m*. Consequently, the subset ***S*** will also be finite and limited to *h*+1 elements. The estimation of heading and velocity from a sequence of points requires operating with finite differences, a technique within the scope of discrete calculus. Velocity is a 2D vector whose norm is the magnitude of the robot forward speed, and whose relation between vector components provides an estimate of the heading. The calculation of velocity implies the use of differentiation, but with discrete data, there is a need to apply *difference equations*, which replace differentiation by taking the difference

between adjacent terms to approximate differential equations. In a Cartesian coordinate system such as the local tangent plane, where the abscissa axis (unit vector $\vec{i}$) represents east and the ordinate axis (unit vector $\vec{j}$) represents north, the position vector $\overrightarrow{P_k}$ of a point *k* is given by Eq. 2.

$$\overrightarrow{P_k} = E_k\ \vec{i} + N_k \vec{j} \qquad [\mathrm{m}] \tag{2}$$

The vector function *distance* $\vec{L}(k,\delta)$ of Eq. 3 provides the Euclidean distance between two points of ***S*** whose indices are separated in the sequence by the calculation step δ. The reference point is *k* and the calculation interval moves back δ positions in matrix $M_s(k)$. Notice that necessarily δ < h, and $\vec{L}(k,\delta)$ is the *backward difference equation* of position vector $\overrightarrow{P_k}$. The *velocity vector* for step δ is given in Eq. 4.

$$\vec{L}(k,\delta) = \overrightarrow{P_k} - \overrightarrow{P_{k-\delta}} = (E_k - E_{k-\delta})\ \vec{i} + (N_k - N_{k-\delta})\ \vec{j} \qquad [\mathrm{m}] \tag{3}$$

$$\vec{V}(k,\delta) = \frac{\vec{L}(k,\delta)}{t_k - t_{k-\delta}} \qquad \left[\mathrm{m \cdot s^{-1}}\right] \tag{4}$$

The forward speed V(k,δ) and the heading H(k,δ) for point *k* can be computed from $\vec{V}(k,\delta)$ through Eqs. 5 and 6 involving the inner product (dot product) of vectors, the norm of a vector, and the trigonometric function arctangent.

$$V(k,\delta) = \left\| \vec{V}(k,\delta) \right\| = \sqrt{\vec{V}(k,\delta) \bullet \vec{V}(k,\delta)} = \frac{\sqrt{(E_k - E_{k-\delta})^2 + (N_k - N_{k-\delta})^2}}{t_k - t_{k-\delta}};\ t_k \neq t_{k-\delta} \tag{5}$$

$$H(k,\delta) = arctg \frac{E_k - E_{k-\delta}}{N_k - N_{k-\delta}};\quad N_k \neq N_{k-\delta};\quad m \geq k > \delta \tag{6}$$

3. Experimental design and setup

A standard tractor was used to reproduce the robot trajectories necessary to accomplish this research. The tractor was equipped with two GNSS receivers setup for providing equivalent NMEA strings. The main receiver was a StarFire iTC^{TM} differential GPS (Deere & Co, Moline, Il, USA) with capabilities to receive licensed signals SF2 and free signals SF1, although all the tests were conducted with the free signal SF1 as most of the local users in Southern Europe are not willing to pay for signal fees. For this situation (SF1), the static accuracy is 75 cm and the pass to pass accuracy is ±33 cm. In addition, a secondary low-cost receiver (Garmin 18x – 5Hz, Olathe, Ks, USA) with an advertised error inferior to 3 m was installed in the cabin of the tractor.

The goal of the experimental design is the acquisition of objective data to help in the design process of robot navigation with regards to GNSS information. In particular, the outcomes of the experiments are meant to rank the parameters of the first row in Table 1. As the use of two receivers per robot is not considered, comparisons were established between GGA-based positions, GGA-based heading and speed, and VTG-based heading (course) and speed over ground. Specific software was developed and customized to the needs of this research, recording GGA and VTG strings simultaneously from both receivers. This software application implemented several filtering routines to enhance the reliability of GNSS data described in detail in Rovira-Más and Banerjee (2013). The heading definition of Eq. 6 is mathematical rather than computational, which in practice leads to stability problems when divisions by zero occur and heading estimates do not vary smoothly in the entire range {0, 360}º. In order to compare heading calculations with direct measurements from VTG messages, Eq. 6 was amplified by the logic set in Table 2.

Table 2. Expanded definition of heading for the practical implementation of Eq. 6.

Condition for membership	H (k, δ) [º]
$E_k \geq E_{k-\delta}$ & $N_k > N_{k-\delta}$	$\frac{180}{\pi} \cdot arctg \frac{E_k - E_{k-\delta}}{N_k - N_{k-\delta}}$
$E_k > E_{k-\delta}$ & $N_k = N_{k-\delta}$	90
$E_k \leq E_{k-\delta}$ & $N_k > N_{k-\delta}$	$360 - \frac{180}{\pi} \cdot arctg \frac{E_{k-\delta} - E_k}{N_k - N_{k-\delta}}$
$E_k < E_{k-\delta}$ & $N_k = N_{k-\delta}$	270
$E_k \leq E_{k-\delta}$ & $N_k < N_{k-\delta}$	$180 + \frac{180}{\pi} \cdot arctg \frac{E_{k-\delta} - E_k}{N_{k-\delta} - N_k}$
$E_k \geq E_{k-\delta}$ & $N_k < N_{k-\delta}$	$90 + \frac{180}{\pi} \cdot arctg \frac{N_{k-\delta} - N_k}{E_k - E_{k-\delta}}$
$E_k = E_{k-\delta}$ & $N_k < N_{k-\delta}$	180

The detailed analysis of the first row of Table 1 unfolds in the set (or family) of tests listed in the first column of Table 3, each of them comprising a number of experiments focused on a determined parameter. Field tests were conducted in 2010, 2011, and 2012, and several farm plots at three different locations were used to acquire the data, one of them barren and all the others planted with grapevines.

Table 3. Experimental design.

Parameter evaluated	Alternatives studied
Receiver type	Low-cost receiver
	High-performance receiver
NMEA string type	GGA-based Heading & Speed
	VTG-based Course & Ground Speed
$M_s(k)$ size for speed calculation	$h = 9$ → Dim ($M_s(k)$) = [10 x 3]
	$h = 5$ → Dim ($M_s(k)$) = [6 x 3]
Threshold velocity for heading calculation	V = 3 km/h
	V = 5 km/h
$M_s(k)$ size for heading calculation	Slow motion (V<5) → $h = 15$ Fast motion (V≥5) → $h = 31$
	Slow motion (V<5) → $h = 9$ Fast motion (V≥5) → $h = 21$

According to Table 3, the first parameter under study is the influence of the receiver specifications on the final outcomes. Normally, high-performance receivers behave more reliably and stably than low-cost devices, but they are not free of external errors such as signal blockage or multipath reflections. This family of tests is devoted to

find out the role that embedded quality indices HDOP (horizontal dilution of precision) and number of satellites play in the early detection of corrupted data. As shown in Table 1, the key navigation parameters heading and speed can be directly read from VTG strings, and alternatively calculated from position and time available in GGA strings. The second set of experiments tries to elucidate if both estimations are really equivalent in terms of precision and reliability, i. e., if they are complementary or redundant. The calculation of heading from GGA positions depends on the forward speed of the robot, and consequently it is important to establish which is the optimal size of Ms(k) for the estimation of speed; a large matrix will introduce a considerable delay, but a small one will yield noisy outcomes. The set of experiments in the third row of Table 3 tries to determine the reasonable size for the speed matrix. The stability of heading calculation according to forward speed (Van Bergeijk et al., 1998; Anderson and Bevly, 2010) advises to adapt the initial equation (Eq. 6) to the speed, but a threshold speed is necessary to classify the motion of the robot according to speed. As farm robots cannot move very fast in off-road terrains, two regimens of low and high speed were established. The fourth set of experiments looks for the boundary limit between high and low speed. Once a limit speed has been fixed, the last family of experiments investigates the size of the sequence of points that best estimates the robot course in real time. As the straight application of Eq. 6 and Table 2 introduces significant noise, a combination of four partial headings with different weights was implemented in the experimental vehicle. Figure 2 illustrates the concept of partial headings for a generic calculation matrix of h elements, and Eq. 7 provides a practical example with $h = 32$ of how partial headings may be weighted in the algorithm.

$$\left.\begin{array}{rcl} H_{\delta 1} & \overset{def}{=} & \delta = 31 : [k-31, k] \\ H_{\delta 2} & \overset{def}{=} & \delta = 9 : [k-9, k] \\ H_{\delta 3} & \overset{def}{=} & \delta = 22 : [k-31, k-9] \\ H_{\delta 4} & \overset{def}{=} & \delta = 7 : [k-12, k-5] \end{array}\right\} \quad H(x) = \frac{2 \cdot H_{\delta 1} + H_{\delta 4}}{3} \tag{7}$$

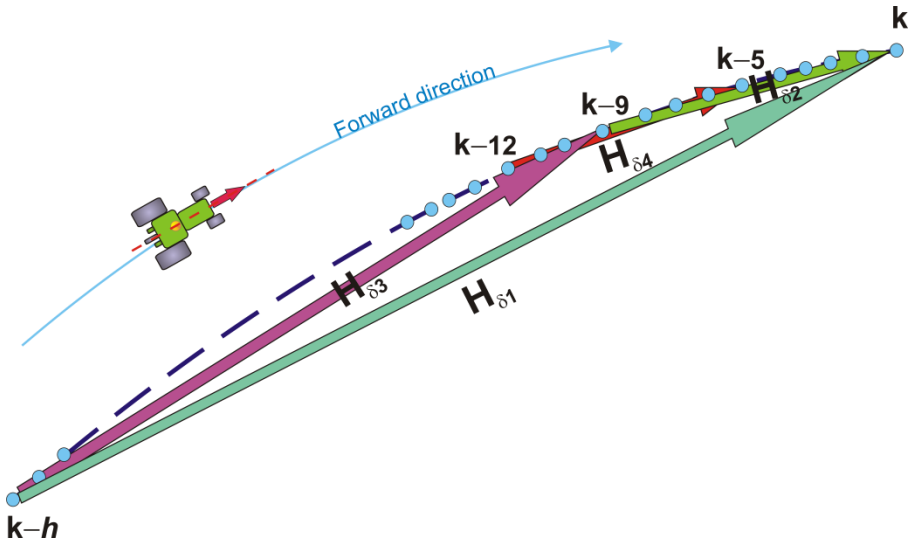

Figure 2. Partial headings in a generic sequence of *h* elements.

5. Results

The hypotheses set in Table 3 were tested in the field over three seasons at a variety of conditions. A summary of the empirical consequences found along the experiments is outlined in Table 4, which includes the principal results and the most representative plots.

Table 4. Summary of field results.

Parameter Evaluated	Field observation	Related figure
Receiver Quality	Helpful but not definitive as fail-safe strategy HDOP and number of satellites not sufficient to grant stability	3
NMEA string Type	At startup; VTG is superior and GGA is slow At headland; GGA is superior and VTG yields wrong estimates	4
Dim ($M_s(k)$) for speed	Positive results around h = 9; h< 9 is less stable and h>9 is too slow	5
$V_{threshold}$ for heading	5 km/h is more stable and accurate than 3 km/h	6
Dim ($M_s(k)$) for heading	Reduced $M_s(k)$ responds faster with negligible initial delay; however, it cannot be adopted for stability reasons	7

Abbreviations: dim→dimension;

The experimental vehicle was setup to simultaneously record the same trajectories using both GNSS receivers (Garmin and StarFire). The objective of this set of tests was to determine the influence of low-precision positioning on vehicle states, especially heading. Figure 3a plots a typical example of low-cost positioning in comparison with the estimates of an accurate GNSS receiver, where errors oscillate in the range 0-10 m. The impact of this positioning imprecision on the calculation of headings is quantified in Figure 3b.

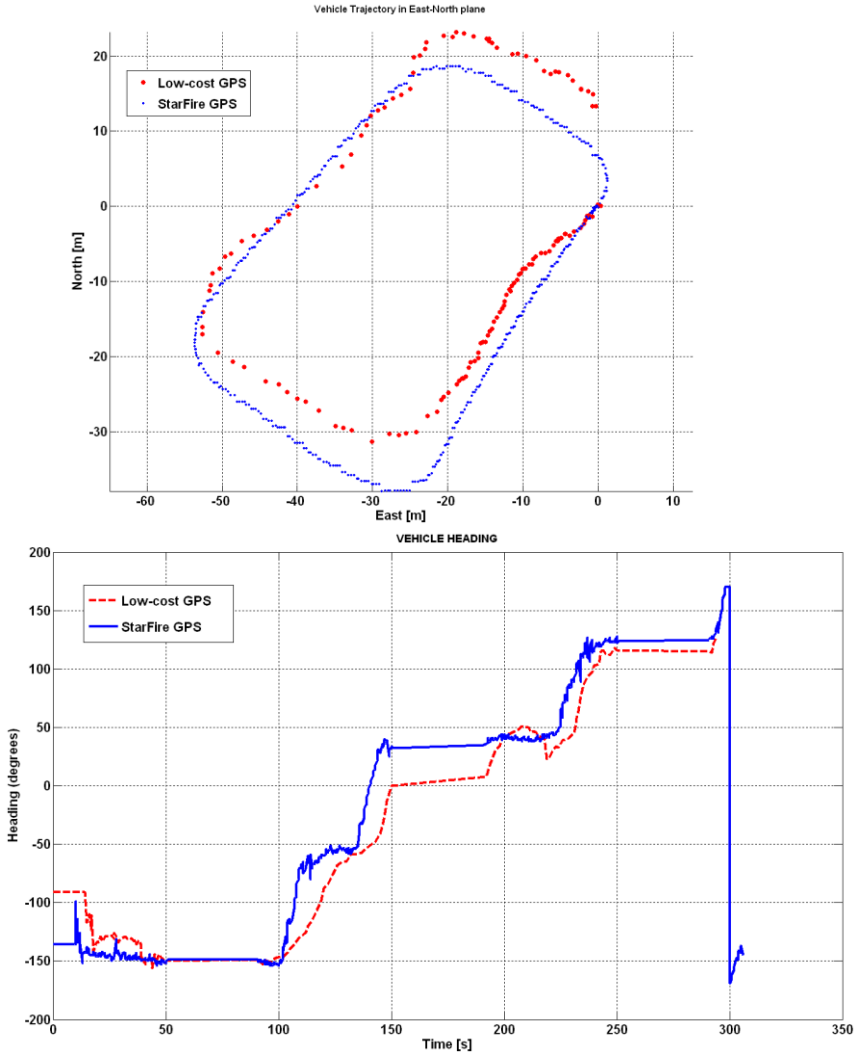

Figure 3. Comparison of receiver performance: east-north plot of tested trajectory (a) and vehicle heading (b).

The measurement of vehicle heading and speed —principal states for robot navigation– were simultaneously recorded with the same receiver (StarFire) by means of

two different techniques: course and Doppler-based velocity contained in VTG strings of the NMEA code; and alternatively heading and forward velocity computed on a sequence of points whose positions are carried in GGA strings of the NMEA code. Figure 4 shows the comparison for two representative tests conducted in different days; a 6-row trajectory recorded in the evening (Fig. 4a) and a 10-row trajectory registered the morning of the following day. Potential local effects on signal quality were considered by repeating the experiments in different days or time of the day from early morning to dusk.

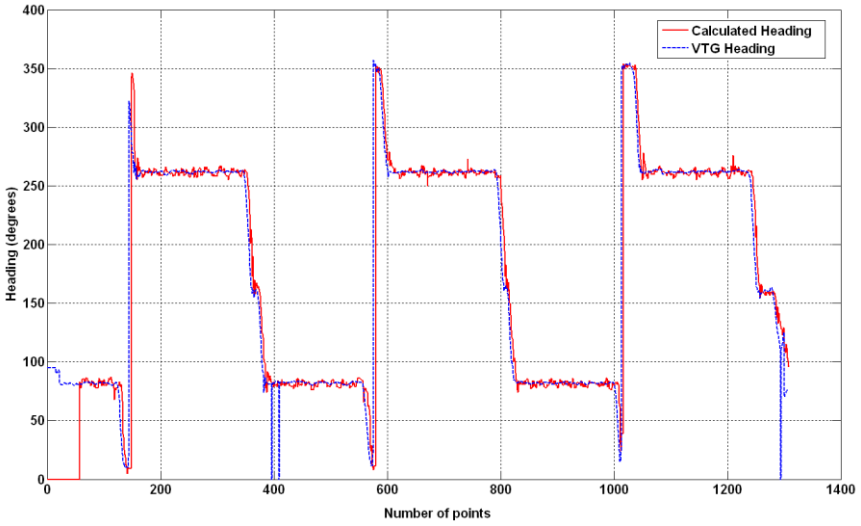

(a)

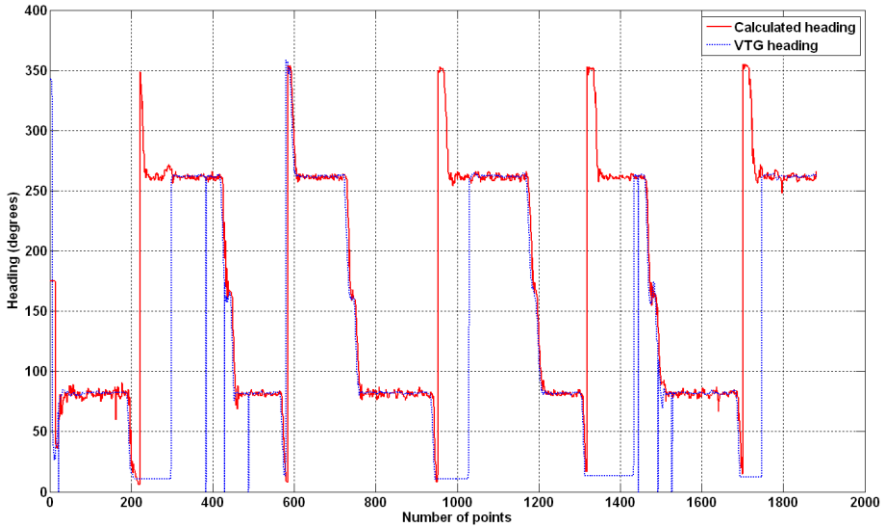

(b)

Figure 4. Comparison of heading read from VTG-based course and calculated from GGA-based positions: 6-row evening test (a) and 10-row morning test (b).

Fixing the optimal size of the matrix $M_s(k)$ used to calculate speed was key for estimating heading and speed from GGA strings as a redundant measurement to VTG

course and velocity. Figure 5 shows the results of downgrading the dimension of $M_s(k)$ from ten points to six points for estimating a target velocity around 4 km/h, usual for a farm robot. VTG measurements are also provided as a ground-truth reference after checking their coincidence with the vehicle's speedometer included in the dashboard. Notice that the number of points evaluated is slightly different as a consequence of different speeds; Fig. 5a plots a faster run and therefore less points were recorded as the GPS frequency was always 5 Hz.

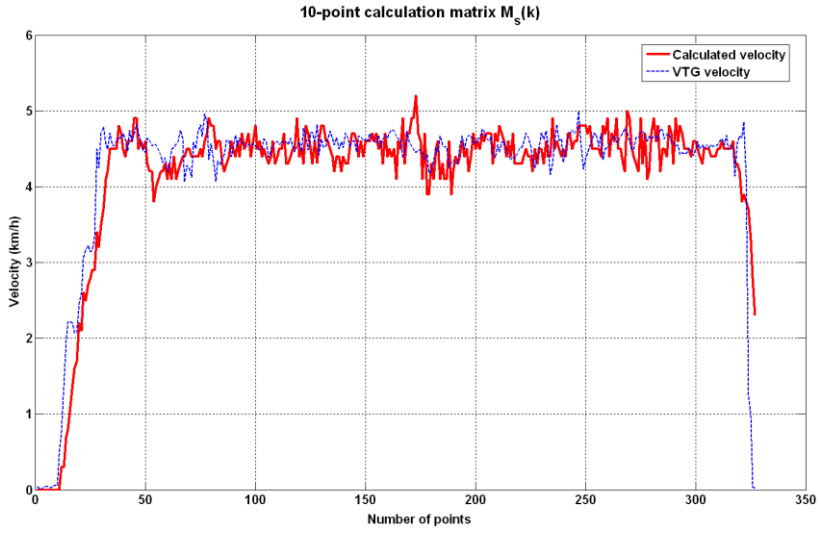

(a)

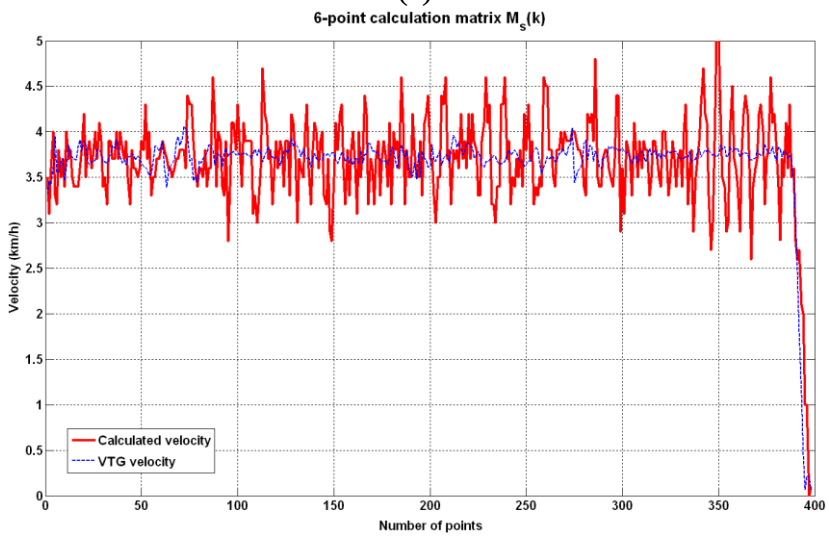

(b)

Figure 5. Influence of calculation matrix dimensions on speed: 10-point matrix (a); and 6-point matrix (b).

The calculation of heading from a sequence of points depends on the robot's

speed. The range of speeds at which farm robots need to operate is limited, normally in the range 0 – 10 km/h. For this situation, it is sufficient to consider two speed ranges, namely slow and fast motion, but the critical point is determining the threshold that classifies the speed of the robot in one of these two classes. Figure 6 depicts the results of the tests devoted to study the size of subset ***S*** for the speed calculation matrix, in particular it shows the effects of lowering the threshold speed from 5 km/h (Fig. 6b) to 3 km/h (Fig. 6a) on heading estimations for a target forward velocity of 3 km/h, very likely in a farm robot. As in previous cases, the VTG course is provided as a reference.

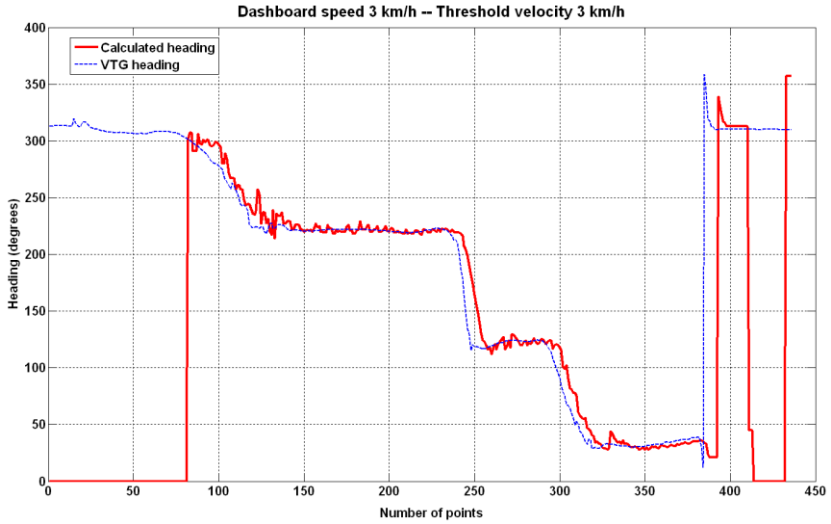

(a)

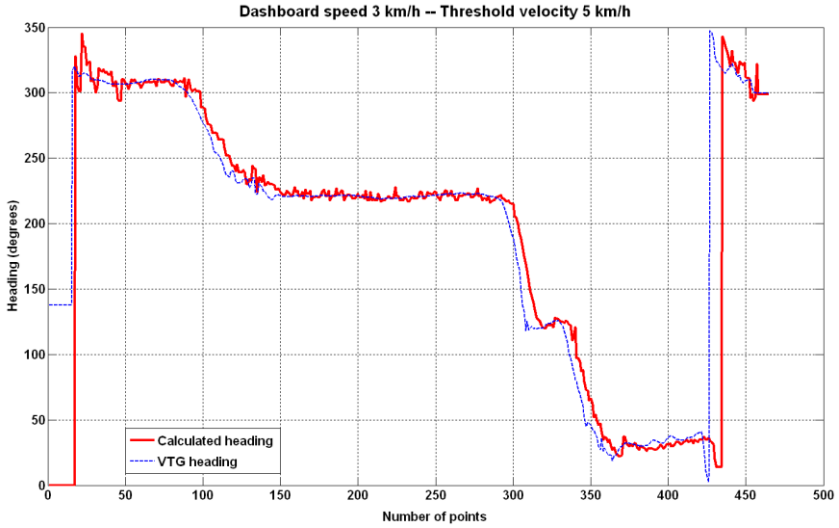

(b)

Figure 6. Influence of threshold velocity V_t on the calculation of robot heading: V_t = 3 km/h (a); and V_t = 5 km/h (b).

The last analysis of this work focused on the dimensions of the calculation matrices for heading estimation, which was different for slow motion and for fast motion according to the selected threshold velocity (5 km/h). The actual size of the calculation matrices determines the particular definition of partial headings $H_{\delta i}$ as illustrated in Fig. 2. Field experience showed that for the range of vehicle speeds considered and a GNSS frequency of 5 Hz, the dimensions proposed in Table 3 provided a general description of the problem. Figure 7 plots the heading calculated when the vehicle moves at 4 km/h and the calculation matrix has 22 points for slow motion and 10 points for fast motion. This plot may be compared with those of figures 3, 4, and 6 which implement matrices of 32 and 16 points for the calculation of headings.

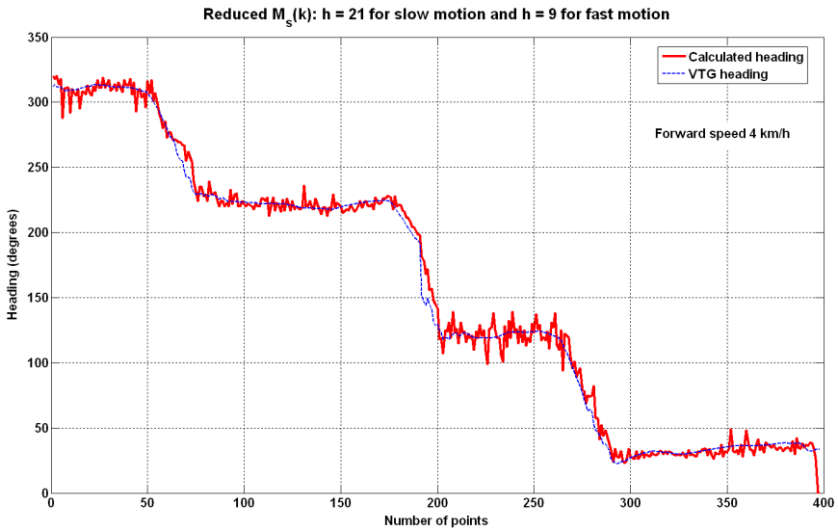

Figure 7. Heading calculated with h = {21, 9} and forward speed of 4 km/h.

6. Discussion

The comparison of receivers led to expected results such as the degradation of the trajectory caused by significant positioning errors, but it also revealed interesting phenomena. In particular, the StarFire trajectory of Fig. 3a shows the east-west drift already noticed by Rovira-Más and Banerjee (2013), and the quality indicators number of satellites and HDOP were surprisingly better for the low-cost receiver (10 satellites versus 9 and HDOP 0.8 – 1 versus constant 1), which in practical terms means that

389 embedded indices are not completely reliable and must be weighted by the quality of each
390 receiver; in other words, low-cost receivers are usually not aware of their inaccurate
391 outputs. In addition, isolated strings of corrupted data were detected over long periods of
392 operation for both receivers, and therefore signal corruption and blockage induced by
393 external conditions such as tall trees and surrounding buildings are always a risk to take
394 into account. Nevertheless, the average performance of the high quality receiver was
395 clearly superior as evidenced by the heading estimation of Fig. 3b, which in reality only
396 yields useful headings for the StarFire system. In light of these results, the selected
397 receiver should be that of highest standards within the assumed cost-efficiency policy,
398 but it will not grant long-run stability unless filtering routines and quality checks are
399 implemented and continuously executed in the navigation engine of the robot.
400 Furthermore, a sophisticated receiver will not grant stability either because multipath
401 reflections, poor constellations, and signal blockages will eventually generate outliers that
402 might create a risk for the navigation of the robot if a contingency plan has not been
403 considered.

404 The fact that heading and velocity can be obtained from the same receiver
405 alternatively from two sources and using different techniques, amplifies the usability of
406 GNSS for robot navigation, as course and speed are basic parameters for setting
407 navigation strategies. The point is whether it makes sense calculating heading and speed
408 from a sequence of points if they are already available in VTG strings of the form
409 established in Fig. 1b. To find it out, several trajectories were followed with the
410 simultaneous recording of heading and speed obtained from both methods. The
411 experimental field consisted of parallel rows of vines spaced 3 m and 130 m long, with a
412 constant heading of 83º when the vehicle traveled east (forward trip) and 263º when
413 traveling west in the return trips. Figure 4a shows the results of the evening test, where

VTG measurements locked the right course from the beginning of the track whereas the calculated headings were delayed in time and did not yield the right course until 50 points were processed. However, the VTG course produced erroneous estimates in the vicinity of point 400, which coincided with a headland turn. A close inspection of embedded quality indices around point 400 reveals a drop in satellites from 9 to 6 together with an increase in HDOP from 1.2 to 2.7. These values for the indices are considered acceptable and do not fully justify the VTG heading drop at the headland. Figure 4b shows the results of a longer test performed in the same scenario the following day, with different atmospheric conditions and ephemeris. The degradation of VTG heading at some —but not all– headland turns is more apparent than in Fig. 4a, and shows that GGA estimates were much more stable than VTG ones. These outcomes are not totally unexpected, because the GNSS accuracy dependency on the travel direction due to satellite geometry was already reported by Wu et al. (2006), and according to Standard X587 (ASABE, 2010), a loss of signal is more common in agriculture at the edge of the fields, and consequently the Standard recommends conducting Dynamic Signal Reacquisition tests on the U-turns of standardized travel courses, reporting heading and speed accuracy separately for straight segments and curved segments. The failures detected at the headland turns with VTG heading (course) and speed advised the redundant estimation of GGA-based navigation states, and justified the analysis of the size of $M_s(k)$ for calculating heading and speed as well as the selection of a threshold velocity between slow and fast motion, discussed in detail in the following paragraphs.

Once the convenience of calculating navigation parameters from a sequence of trajectory points has been proved, the size of the sets of points (subset $\boldsymbol{S}$) used in the calculation must be determined as it will impact the final outcomes. The dimension of the calculating matrix will be different for speed, slow motion heading, and fast motion

439 heading, being speed especially important because it determines the size of the calculation
440 matrices used for the estimation of heading. Extensive testing revealed that a calculation
441 matrix of ten rows (h = 9) resulted in reasonable estimates. However, the initial delay
442 could be eliminated with a smaller matrix allowing for faster cycles. To check such
443 assumption, speed estimation was carried out with a reduced matrix of six elements (h =
444 5), as compared in Fig. 5. For common speeds of approximately 4 km/h, Fig 5a shows
445 that h = 9 produces more stable outcomes than a matrix considering six points (Fig. 5b).
446 Heading calculations require the application of different equations according to
447 forward speed, which in practical terms implies the selection of three basic parameters:
448 the threshold speed that separates slow motion from fast motion, and the dimensions of
449 the calculation matrices for each type of motion, which in turns leads to a differentiated
450 definition of partial headings as generally indicated in Fig. 2. Being 4 km/h a reasonable
451 operating speed for a farm robot, two boundary speeds of 3 km/h and 5 km/h were
452 analyzed as thresholds between the slow motion class and the fast motion class. Fig. 6
453 shows greater stability for the 5 km/h threshold (6b), especially at initiation where the
454 lower threshold is affected by a significant delay (6a). For both estimates there exists a
455 slight delay with respect to VTG values, which become very resourceful as a redundant
456 check to measure the stability of calculated heading. The attenuation of noise in the
457 calculation of heading required the use of large matrices, which eventually resulted in
458 important delays, mainly if compared to VTG estimates. Although satisfactory results
459 were achieved with sequences of 32 elements in fast motion and 16 elements in slow
460 motion, if the same response could be granted with a significant reduction in the size of
461 the sequence, such response would be faster and more promptly available. To prove so,
462 the fast motion matrix was downgraded to 22 elements whereas the slow motion matrix
463 was reduced to 10 points. Unfortunately, Fig. 7 indicates that for a usual speed of 4 km/h,

464 the reduction in the number of elements for estimating heading leads to less stable results
465 when compared to figures 3, 4, and 6, where headings were calculated with the larger
466 matrices. The results found along the experiments, and summarized in Table 4, were
467 implemented in the experimental vehicle according to the block diagram of Fig. 8. Notice
468 that for this application, speeds below 0.5 km/h were disregarded as noise, and speed
469 discrimination occurred at 5 km/h. This flow chart provides a practical example of the
470 role of GNSS in the navigation strategies of farm robots, but other specific applications
471 will likely require other definition and combination of partial headings, or calculation
472 matrices of different dimensions, even though the philosophy is valid for a wide variety
473 of agricultural moderate-size robots.

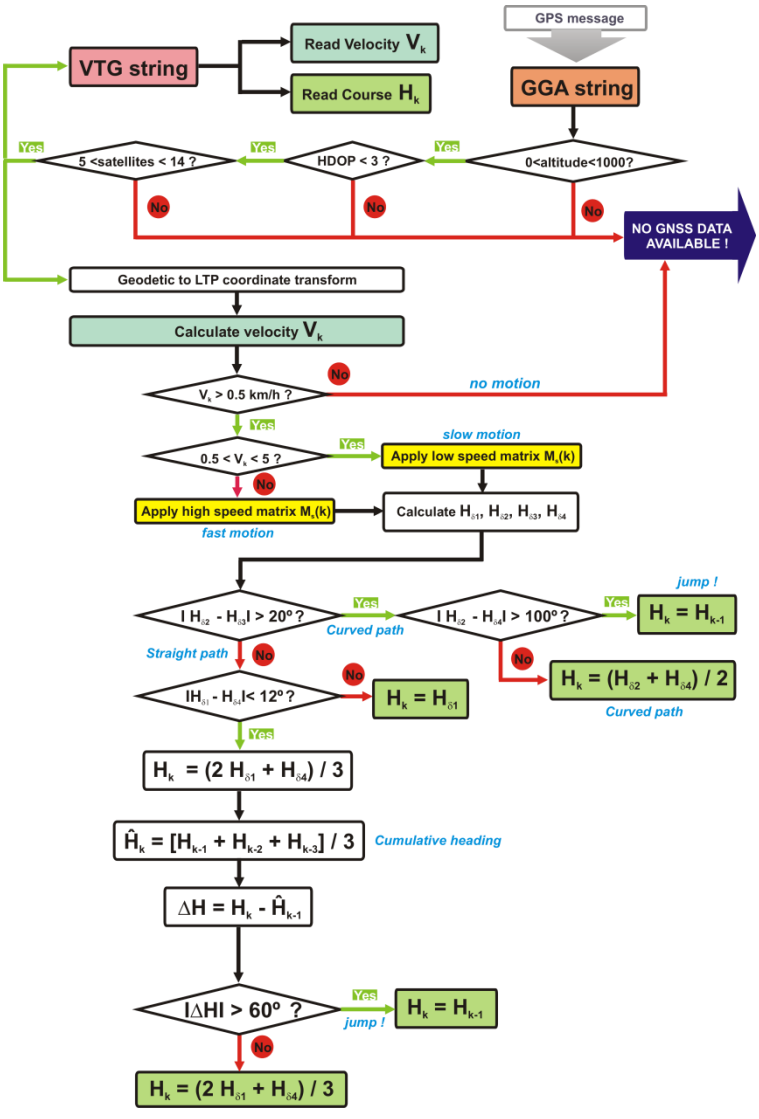

474

Figure 8. Block diagram of GNSS algorithm implemented in the vehicle.

7. Conclusions

This research intended to outline the role of GNSS in cost-efficient farm robots, especially in terms of navigation. Results showed that it is always convenient to integrate GNSS in this kind of robots, but this integration can never be *plug-and-play*; on the contrary, it requires the careful filtration of data in such a way that spurious information never enters the processing loop of the navigation engine. The accuracy of the GNSS receiver has a positive impact in the mobility of the robot, but it cannot grant long-term stability in agricultural fields where multipath reflections and signal blockage are unpredictable. As a result, GNSS-borne data requires redundancy and continuous fail-safe checking. This redundancy may be achieved both within GNSS data and from external sensors. The former implies the concurrent analysis of VTG and GGA strings whereas the latter requires the implementation of alternative sensors such as compasses, radars, or optical devices. The experiments conducted showed that GGA and VTG information is complementary rather than substitutive, given that VTG course and speed is accurate at startup but becomes unreliable at the headland turns where GGA-derived heading and speed is stable. Nevertheless, in order to get accurate heading and speed from a sequence of points defined by GGA strings, important decisions must be made regarding the primary parameters of the calculation algorithm. In particular, the size of the calculation matrices and the strategy to deduce stable estimates from a sequence of points defining the robot's path is essential to make the most efficient use of GNSS. Overall, GNSS is a key component of farm robots for the cost-efficient redundant information that it provides. The conceptual scheme of Fig. 9 summarizes the role of GNSS in farm robots, with the redundant estimation of critical navigation parameters. Dashed lines in pale ink represent a potential augmentation of the navigation system as long as it is compatible

with the assumed cost-efficiency policy. There exists a substantial difference between cost-efficiency robots and low-cost GNSS. Whether low-cost GNSS devices can help with the design of cost-effective agricultural robots is a relevant question, and the key is on reliability rather than cost as long as cost-efficiency requirements are met. As a result, RTK devices and subscription fees will not be helpful in general terms, but the ideal cost for the receiver will depend on the final cost fixed for the robot and the safety standards established for the tasks programmed in the robot. The smart implementation of GNSS will definitely result in the smart behavior of agricultural robots.

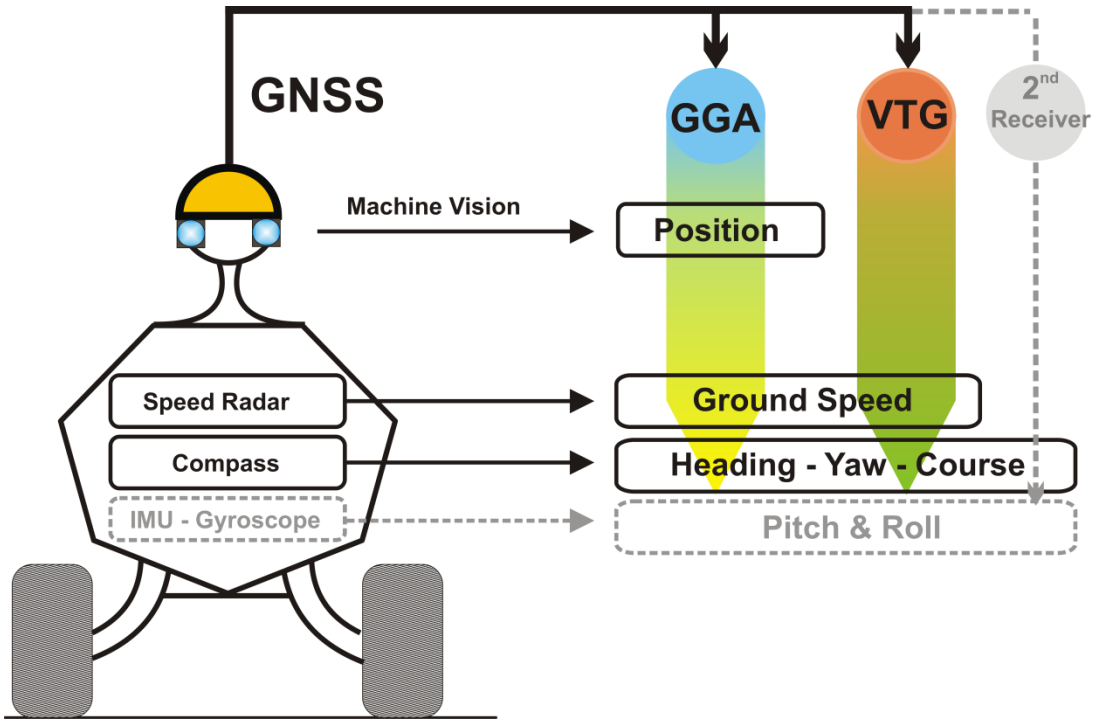

Figure 9. Role of GNSS in the navigation engines of farm robots.

References

Anderson, R., Bevly, D. M., 2010. Using GPS with a model-based estimator to estimate critical vehicle states, Vehicle System Dynamics 48 (12): 1413 – 1438.

ASABE, 2010. Dynamic testing of satellite-based positioning devices used in agriculture. Standard X587 (Draft 10), Available from http://elibrary.asabe.org. [Accessed on 3 December 2012]

516 Chosa, T., Omine, M., Itani, K., 2007. Dynamic performance of global positioning system
517 velocity sensor for extremely accurate positioning, Biosyst. Eng. 97: 3–9.
518 Cocco, L., Rapuano, S., 2007. Accurate speed measurement methodologies for
519 Formula One cars, in: Proc. IEEE Instrumentation and Measurement Technology
520 Conference, Warsaw, Poland.
521 Ding, W., Wang, J., 2011. Precise velocity estimation with a stand-alone GPS receiver.
522 Journal of Navigation 64: 311-325.
523 Emmi, L., González-de-Soto, M., Pajares, G., González-de-Santos, P., 2014. Integrating
524 Sensory/Actuation Systems in Agricultural Vehicles. Sensors 14(3): 4014-4049.
525 Joerger, M., Pervan, B., 2006. Autonomous ground vehicle navigation using integrated
526 GPS and laser-scanner measurements, in: Proc. of Position, Location, and
527 Navigation Symposium (PLANS), San Diego, CA, 2006, pp. 988–997.
528 Kondo, N., Monta, M., Noguchi, N., 2011. Agricultural Robots: Mechanism and
529 Practices. Trans Pacific Press, Balwyn North Victoria, Australia.
530 Nørremark, M., Griepentrog, H. W., Nielsen, J., Søgaard, H. T., 2008. The development
531 and assessment of the accuracy of an autonomous GPS-based system for intra-
532 row mechanical weed control in row crops, Biosyst. Eng. 101: 396– 410.
533 Rovira-Más, F., 2009. Recent innovations in off-road intelligent vehicles: in-field
534 automatic navigation, Recent Patents on Mechanical Engineering 2: 169–178.
535 Rovira-Más, F., 2010. Sensor architecture and task classification for agricultural
536 vehicles and environments. Sensors 10: 11226-11247; doi:10.3390/s101211226
537 Rovira-Más, F., Zhang, Q., Hansen, A. C., 2010. Mechatronics and Intelligent Systems
538 for Off-road Vehicles. Springer, London, pp. 68 – 71.
539 Rovira-Más, F., Banerjee, R., 2013. GPS data conditioning for enhancing reliability of
540 automated off-road vehicles, J. Automobile Eng. 227 (4): 78 – 92.

541 Serrano, L., Kim, D., Langley, R. B., Itani, K., Ueno, M., 2004. A GPS velocity sensor:
542 how accurate can it be?- A first look, in: Proc. of ION National Technical
543 Meeting, San Diego, CA, 2004, pp. 875–885.
544 Van Bergeijk, J., Goense, D., Keesman, K. J., Speelman, L., 1998. Digital filters to
545 integrate global positioning system and dead reckoning. J. Agric. Eng. Res. 70:
546 135–143.
547 Wu, C., Ayers, P. D., Anderson, A. B., 2006. Influence of travel direction on GPS
548 accuracy for vehicle tracking, Transac. ASABE 49(3): 623 – 634.
549
550
551
552